HHS Public Access

Author manuscript

Integr Biol (Camb). Author manuscript; available in PMC 2017 November 07.

Published in final edited form as:

Integr Biol (Camb). 2016 November 7; 8(11): 1170–1182. doi:10.1039/c6ib00192k.

Mitochondrial respiration is sensitive to cytoarchitectural breakdown

Judith Kandel[a,#], **Alessia A. Angelin**[b], **Douglas C. Wallace**[b,c], and **David M. Eckmann**[a,d,e,*]

[a]Department of Bioengineering, University of Pennsylvania, Philadelphia, PA 19104

[b]Center for Mitochondrial and Epigenomic Medicine, Children's Hospital of Philadelphia

[c]Department of Pathology and Laboratory Medicine

[d]Department of Anesthesiology and Critical Care, Perelman School of Medicine

[e]Institute for Medicine and Engineering, University of Pennsylvania, Philadelphia, PA 19104

Abstract

An abundance of research suggests that cellular mitochondrial and cytoskeletal disruption are related, but few studies have directly investigated causative connections between the two. We previously demonstrated that inhibiting microtubule and microfilament polymerization affects mitochondrial motility on the whole-cell level in fibroblasts. Since mitochondrial motility can be indicative of mitochondrial function, we now further characterize the effects of these cytoskeletal inhibitors on mitochondrial potential, morphology and respiration. We found that although they did not reduce mitochondrial inner membrane potential, cytoskeletal toxins induced significant decreases in basal mitochondrial respiration. In some cases, basal respiration was only affected after cells were pretreated with the calcium ionophore A23187 in order to stress mitochondrial function. In most cases, mitochondrial morphology remained unaffected, but extreme microfilament depolymerization or combined intermediate doses of microtubule and microfilament toxins resulted in decreased mitochondrial lengths. Interestingly, these two particular exposures did not affect mitochondrial respiration in cells not sensitized with A23187, indicating an interplay between mitochondrial morphology and respiration. In all cases, inducing maximal respiration diminished differences between control and experimental groups, suggesting that reduced basal respiration originates as a largely elective rather than pathological symptom of cytoskeletal impairment. However, viability experiments suggest that even this type of respiration decrease may be associated with cell death.

[*]To whom correspondence should be addressed: Department of Anesthesiology and Critical Care, 27B John Morgan Building, 3620 Hamilton Walk, Philadelphia, PA 19104, USA. Tel: 215-746-1482, David.Eckmann@uphs.upenn.edu.

[#]Current address: Complete Healthcare Communications, Inc, One Dickinson Drive, #200, Chadds Ford, PA 19317

AUTHOR CONTRIBUTIONS

All authors were important in designing the experiments. JK and AAA performed the experiments. JK analyzed the data with contributions from AAA. JK wrote the paper with critical suggestions from AAA, DCW and DME. DME advised the work.

DATA AVAILABILITY

All data is available on Figshare via the following links: https://figshare.com/s/67d71f71c1792498185f (fluorescent images), https://figshare.com/s/7e4dc6e360753df695be (Seahorse XF Analyzer data) , and https://figshare.com/s/38783bd3357ad8b0c396 (MATLAB codes).

INTRODUCTION

Cellular pathology is often assumed to be reflected by either mitochondrial or structural alterations, whereas in reality the two often appear in parallel. In the mitochondrial realm, diseased cells show changes in metabolic pathways[1,2], respiration rates [3,4], reactive oxygen species generation [3,5], and even mitochondrial morphology [6,7] or motility [8,9]. On the other hand, damaged cytoarchitecture can manifest as changes in cell shape [10], traction force generation [11], or stiffness of the extracellular matrix [12,13] or the cell itself [14,15]. While the pathways involved in both mitochondrial and mechanical dysfunction are individually complex, there are abundant suggestions in the literature that there are multiple links between them. Here we examine the mitochondrial consequences of cytostructural impairment. This work builds upon our previous research characterizing the effects of cytoskeletal toxins on mitochondrial motility in particular [16].

For decades, mitochondria have been known to be structurally linked to microtubules [17], and microtubule breakdown impairs mitochondrial motility [16,18]. Associations between mitochondria and actin filaments, which are largely responsible for cellular mechanics [19], have mostly been studied in yeast [20], but recent work indicates that actin is involved in mitochondrial motility [16] and fission [21] in mammalian cells. Beyond structure and motility, studies indicating functional links between mitochondria and the cytoarchitecture are often predicated on the observation that mitochondria tend to localize to energy-requiring areas of the cell, such as the growth cones of neuronal axons [22] and viral assembly sites in infected cells [23]. Two examples include mitochondrial localization at the periphery of a freshly plated cell [24], which presumably locally provides energy for cell spreading, and the correlation of mitochondrial inner membrane potential with cellular projection area during early phases of cell spreading [25]. Similarly, one report demonstrated elevated mitochondrial inner membrane potentials in cells at the edge of a migrating sheet [26], and others have even shown increased mitochondrial inner membrane potential at the periphery of more stationary cells [27], where traction forces are usually highest [11]. Additional studies have demonstrated directed mitochondrial localization during migration of lymphocytes [28] and cancer cells [29]. While intriguing, these studies are limited to observations regarding subcellular localization and energetic potential of mitochondria, and fall short of directly examining the interplay between cytoarchitectural integrity and mitochondrial function.

Here, we analyzed the direct effects of cytoskeletal inhibitors on mitochondrial inner membrane potential, morphology, and oxygen consumption in intact, adherent human dermal fibroblasts. Earlier work suggests that endothelial cells rely on glycolysis, rather than oxidative phosphorylation, to provide ATP for actin stress fiber maintenance [30], but this is consistent with general glycolytic dependence of endothelial cells [31]. Our current work investigates whether oxidative phosphorylation may be more important for cytoskeletal maintenance in fibroblasts. Decreased inner membrane potential is perhaps the clearest sign of mitochondrial injury and thus represents an obvious first step to assessing mitochondrial health in response to impending damage. We also considered mitochondrial morphology since it is often, but not always, linked to energetic state [32]. Finally, we assessed whether cytoskeletal toxins induced changes in mitochondrial oxygen consumption rates, which may

indicate whether mitochondrial energetics are maintained or compromised. Overall, our work shows that while membrane potential remains intact, cytoskeletal breakdown can alter mitochondrial respiration by itself or in concert with known mitochondrial stressors. Our results further suggest that mitochondrial shortening may counteract the effects of cytoskeletal toxins on mitochondrial respiration.

MATERIALS AND METHODS

Cell culture and reagents

Adult human dermal fibroblasts between passages 1 and 5 (Lifeline Cell Technology, Walkersville, MD) were cultured in FibroLife cell culture media (Lifeline Cell Technology) as previously described [16]. Cells were seeded approximately 48 hours prior to experiments.

For experiments involving measuring changes in mitochondrial inner membrane potential and mitochondrial morphology, cells were plated on MatTek 35-mm glass-bottom dishes (MatTek, Ashland, MA) at a density of ~25,000 cells/dish. Dishes were coated for 30-40 minutes with 10 μg/mL fibronectin (BD Biosciences, San Jose, CA) dissolved in PBS prior to cell plating. For oxygen consumption measurements, cells were plated in 24-well plates (Seahorse Biosciences, North Billerica, MA) at a density of ~10,000 cells/well. This concentration was determined to result in a confluent monolayer at the time of experiments. For cell viability experiments, cells were seeded on standard tissue-culture treated 24-well plates (Corning, Corning, NY) at a density of 50,000/well.

Assessing changes in mitochondrial inner membrane potential and morphology

Changes in mitochondrial inner membrane potential and morphology in single cells were assessed using wide-field fluorescence microscopy as previously described [16]. Cell viability was also measured using this setup. This system employed a QImaging QIClick camera (QImaging, Surrey, BC, Canada) (1x1 binning, 1392x1040 pixels) attached to an Olympus IX70 microscope (Olympus, Melville, NY) with an Olympus 40x oil immersion objective lens (Olympus) and Photofluor light source (89 North, Burlington, VT). Computer control of the microscope was facilitated by LUDL programmable filter wheels, shutters, and focus control (LUDL Electronic Products, Hawthorne, NY) and images were collected using IPL 3.7 software (BD, Rockville, MD). For each experiment, cells were visualized using standard TRITC and FITC filters.

The day before experiments, cells were transfected with CellLight Mitochondria-GFP, BacMam 2.0 (Life Technologies, Grand Island, NY) at a concentration of 40 particles per cell, and kept in the dark at 37°C. Several hours before experiments, cells were also dye-loaded with 20 nM Tetramethylrhodamine methyl ester (TMRM, Life Technologies), a mitochondrial potential dye, for 60 minutes at room temperature in the dark. After rinsing, cells were placed in Recording HBSS (HBSS pH 7.4 with 1.3 mM $CaCl_2$, 0.9 mM $MgCl_2$, 2 mM glutamine, 0.1 g/L heparin, 5.6 mM glucose, and 1% FBS) for imaging.

In each experiment, a selected cell was first imaged in both the mitoGFP and TMRM channels in recording HBSS. At T=0, recording HBSS was removed from the dish and

replaced with either recording HBSS (control), recording HBSS containing 5 μL/mL DMSO, or recording HBSS containing a given cytoskeletal toxin. The DMSO concentration was equivalent to the highest concentration of drug stock solution for which a morphology effect was observed, and was performed in order to ensure that no observed effects resulted from the DMSO solvent rather than the cytoskeletal drugs. Cytochalasin D (cytD) was taken from a stock solution of 1 mM in DMSO and nocodazole (noco) was taken from a stock solution of 10 mM in DMSO. The cell was then imaged again in both channels at T=30 minutes. Data for each experimental group were collected over two or more days, for a total of 7-22 cells per group. Cytoskeletal toxins were confirmed to be working using Alexa Fluor 546 phalloidin (Life Technologies; for cytD) and TubulinTracker (Life Technologies; for noco) dyes (previously shown in [16]).

Images from the mitoGFP channel were preprocessed using ImageJ as previously described [16]. Briefly, images were first convolved using a 5x5 edge detection filter (Process>Filters>Convolve). The resulting image was then bandpass filtered (Process>FFT>Bandpass Filter…) between 2 and 100 pixels. Finally, the image was manually thresholded (Image>Adjust>Threshold) by eye at a level which removed random background pixels in order to maximize signal and minimize noise. Before applying the chosen threshold value, a mitochondrial region of interest (ROI) was first generated by creating a selection (Edit>Selection>Create Selection) and then adding this to the ROI manager (Analyze>Tools>ROI Manager>Add[t]). The threshold was then applied. Figure 1a(iv) shows the resulting image for a sample cell.

Mitochondrial inner membrane potential was measured by opening the TMRM channel image in ImageJ and superimposing the corresponding mitoGFP processed image ROI onto it (by selecting the ROI in ImageJ). Figs 1b(iv) and 1c(iv) show examples of mitochondrial ROIs superimposed onto corresponding TMRM images. Since the mitoGFP fluorescence results from transfection, it does not depend on inner membrane potential, and thus allows for mitochondrial identification even when mitochondria have depolarized as in the case of CCCP treatment. Fluorescence intensity within the mitochondrial ROI was then measured (Analyze>Measure) for a mean TMRM fluorescence within the mitochondrial region of the cell. This process was repeated for the same cell 30 minutes following drug exposure, and the resulting mean fluorescence was normalized to the corresponding value prior to treatment. 5 μM CCCP was used as a positive control (Figure 1b-c, Figure 2).

Object recognition functions in Matlab R2010a (Mathworks, Natick, MA) were applied to the preprocessed image of each cell at each time point (Figure 1a(iv)) in order to assess mitochondrial morphology. The code constructed for this purpose is publicly available online. Briefly, *bwconncomp* was used to find the mitochondrial objects in each image (using 8-pixel connectivity) followed by *regionprops*, which measured the area of each object. The noise floor was set at 5 pixels, and objects with areas less than this were discarded. The image was then reconstructed without these objects. *Bwboundaries* was used to find mitochondrial objects in the new image, and *regionprops* measured various attributes of these objects including major axis length. Since lengths were not normally distributed, the metric used to assess overall mitochondrial length at a given time point was the geometric mean. The geometric mean of mitochondrial length was then calculated for each cell

following treatment, and normalized to the geometric mean of the same cell prior to treatment. The number of mitochondrial objects detected in each reconstructed image was calculated using *bwboundaries*.

Oxygen consumption measurements

Prior to beginning respiration measurements, cells were pre-treated for 30 minutes as indicated with DMSO, cytD, noco or a combination thereof. Some cells were pre-treated prior to the addition of cytoskeletal toxins with 100 nM A23187 (A23; taken from a stock solution of 2 mM) for 20 minutes. This concentration was chosen based on the lack of effect on respiration at this concentration. After 20 minutes, A23-containing media was removed and replaced with media containing both A23 and appropriate cytoskeletal toxins. Control DMSO groups included a low DMSO concentration and a high DMSO concentration. The low DMSO concentration was 0.2 μL/mL (equivalent to the lowest concentration of noco or cytD stock used) while the high DMSO concentration was 10.05 μL/mL (equivalent to the highest load of DMSO from stock used, in the 50 μM noco + 5 μM cytD + A23 group). These controls were slightly different from those used for morphology and potential measurements, and were chosen to correspond to the lowest and highest DMSO concentrations for which an OCR effect was observed. Control cells (without DMSO) were maintained in their original media.

Mitochondrial oxygen consumption rates (OCR) were evaluated in intact, adherent cells using the Seahorse XF24 Analyzer (Seahorse Bioscience, Billerica, MD). The experiments were performed with unbuffered DMEM XF assay media supplemented with 2mM GlutaMAX, 1mM sodium pyruvate, and 5mM glucose (pH 7.4 At 37°C). The mitochondrial respiration was measured before any pharmacological perturbation (basal respiration). Cells were then subjected to 1 μg/ml oligomycin (oligo) to measure proton leak, followed by 0.4 μM FCCP to induce maximal respiration. Finally, 1 μM rotenone followed by 1.8 μM antimycin A was applied in order to inhibit all mitochondrial respiration. In each experiment, 3 wells were left unseeded to serve as background measurements. Each experimental condition was applied to 4-6 wells per plate, and repeated over 3-4 days for a total of 12-24 wells per group.

Basal respiration was measured at three consecutive time points, as was respiration following application of each oligo, FCCP, rotenone and antimycin. These three values were averaged to give a single measure of respiration for each state for each well. Outliers were excluded on the basis of one or more visual criteria (1) OCR did not respond to stimulation with FCCP, visually showing a flat line; (2) OCR (basal, oligo, FCCP, rotenone, or antimycin) was visually well below background well readings; (3) Basal OCR visually lay well below antimycin readings for the same well. The latter two categories rarely occurred. More often, a fourth category was invoked, which considered wells which appeared to have readings significantly different from other wells in the same group from the same day. The OCR readings from these wells were subjected to Grubb's test using a freely available online calculator (http://graphpad.com/quickcalcs/grubbs2/) to assess whether they were outliers, using either basal OCR or OCR following addition of a mitochondrial inhibitor. Significance was set at $p < 0.05$, and wells meeting this criterion were excluded from

analysis. Background readings for each plate were calculated by averaging the OCRs from the background wells for those plates, and subtracted from all subsequent readings. Erratic or extreme background well readings were excluded from this calculation. Prior to data analysis, the OCR from each well after antimycin addition was subtracted from the corresponding basal, oligo and FCCP rates in order to report only mitochondrial OCRs. Each well was considered to be a separate experiment, and data are presented as the mean ± standard deviation for all experiments.

Cell viability experiments

Two days after seeding, cells were dyed with 10 μg/mL Hoechst 33342 (Life Technologies) diluted in Recording HBSS for 30 minutes at room temperature protected from light. After rinsing, cells in each well were imaged in Recording HBSS containing 1 μg/mL propidium iodide (PI; Life Technologies). All drugs were dissolved in HBSS containing this concentration of PI. Select wells were pretreated with 100 nM A23, and were then imaged 20 minutes following this treatment. HBSS from all wells was then replaced with HBSS containing applicable drugs, with the A23-pre-treated cells given drugs containing 100 nM A23. Cells were imaged with a 10x lens in the DAPI and TRITC channels at 30 minutes and 3 hours following drug treatment. Exposure times were kept constant at each time point but sometimes were increased for later time points due to photobleaching. Each experimental group was tested in 2-3 wells per day, repeated over 2-3 days. Three images per well per time point were taken.

Data analysis and statistics

Matlab was used for pairwise t-tests comparing each experimental group to the control group in order to test for significance of a given experimental outcome. For oxygen consumption measurements, all wells from a given experimental group were compared to all wells from the control group (without DMSO). R was then used for adjusting p-values for multiple comparisons (*p.adjust*) using the Benjamini-Hochberg method. P-values were adjusted for all comparisons to a given control group. The p-values are generally accepted as significant when $p < 0.05$.

RESULTS

Mitochondrial potential is unchanged following treatment with cytoskeletal toxins

Figure 1 demonstrates how dual staining was used to measure changes in mitochondrial inner membrane potential. MitoGFP staining was used to create a mitochondrial ROI which allowed us to measure TMRM fluorescence only within the mitochondrial boundaries.

Control cells exhibited a ~30% decrease in TMRM fluorescence after 30 minutes (Figure 2). This decrease is probably due in part to the photosensitivity of TMRM [33], which leads to bleaching under the intense illumination transmitted through the oil-immersion lens. Additionally, replacing the medium with either control or drugged media likely leads the dye to redistribute between the cells and the culture dish, exiting the mitochondria and contributing to the observed decrease in TMRM fluorescence. This decrease likely does not

indicate significant mitochondrial depolarization, as CCCP addition results in a much more drastic decrease in TMRM signal.

Compared to control cells, none of the cytoskeletal toxins used resulted in significant reductions in mitochondrial inner membrane potential. In two cases (nocodazole 50 μM and noco 50 μM + cytD 5 μM), there was suprisingly less of a TMRM fluorescence decrease than in control cells ($p < 0.05$). This observation may indicate a slight hyperpolarization in comparison to normal cells, but more likely indicates that these cells randomly exhibited fewer effects of photosensitivity and/or dye redistribution than other cells. Alternatively, 50 μM noco could result in a membrane potential increase reflecting a major reduction in cellular bioenergetics (see data from oxygen consumption measurements below). Over the 30 minute drug exposure used in this experiment, the electron transport chain would continue to operate, since oxygen is not limiting. Without ADP to be rephosphorylated at the expense of the electrochemical gradient, the electrochemical gradient would rise accounting for the high membrane potential at 50 μM versus 10 μM. Overall, these data suggest that the cytoskeletal toxins used have no depolarizing effect on mitochondria. However, less extreme mitochondrial effects should not be discounted. We therefore examined the effects of these toxins on mitochondrial morphology and respiration.

Specific cytoskeletal toxins induce shortening of mitochondria

Analysis of mitochondrial morphology was based on mitoGFP staining. MitoGFP images from each time point were processed in order to generate images clearly showing mitochondria within the cell (Figure 1a-c(iv>)).

In most cases, mitochondrial lengths remained unchanged following treatment with cytoskeletal toxins (Figure 3a). However, mitochondrial lengths significantly decreased when cells were exposed to 5 μM cytD, or a combined dose of 10 μM noco + 1 μM cytD. Surprisingly, mitochondrial lengths did not change when cells were subjected to 50 μM noco + 5 μM cytD. This observation suggests that mitochondrial shortening is not directly related to the change in cell shape induced by high concentrations of cytD.

Figure 3b shows an example of a cell subjected to 5 μM cytD exhibiting mitochondrial shortening. Panel (i) shows the mitoGFP channel of the cell prior to treatment, while panel (ii) shows the same cell after 30 minutes of exposure to 5 μM cytD. In this case, the geometric mean of mitochondrial lengths decreased by approximately 25% following cytD treatment.

We also evaluated changes in numbers of mitochondria in all experimental groups in order to assess whether mitochondrial shortening was indicative of fragmentation. As Figure S1 shows, none of these groups showed alterations in mitochondrial number per cell following cytoskeletal inhibition that differed from control cells. This indicates that mitochondria in the 5 μM cytD and 10 μM noco + 1 μM cytD groups probably do not undergo fragmentation as a result of cytoskeletal toxicity.

Cytoskeletal toxins caused decreased cellular basal oxygen consumption rates

Next, we measured oxygen consumption rates (OCRs) to assess whether mitochondrial function was perturbed in intact cells subjected to various cytoskeletal inhibitors. Figure 4a shows grouped experimental results from a typical trial, with outliers removed. Figure S2a shows the raw data from the same experiment before outliers were removed for the purposes of analysis, and Figure S2b shows the raw data with outliers omitted. This experiment clearly demonstrates that the noco 50 μM + A23 group group exhibits lower basal oxygen consumption rates than any of the other groups measured.

Both high and low concentrations of DMSO were confirmed to not affect mitochondrial respiration (Figure 4b(i)). Experimental groups were therefore compared to the controls (which were not treated with DMSO) for purposes of uniformity. OCR following antimycin addition was subtracted for each experimental well before analysis in order to only consider mitochondrial respiration. In many cases, exposure to cytoskeletal toxins decreased basal respiration, either trending towards or achieving significance (Figure 4b(ii-iv)). The most significant decrease was shown by the noco 50 μM + cytD 5 μM group, which showed a basal OCR of 34.42 ± 14.22 pmol/min as compared to the control basal OCR of 59.86 ± 23.17 pmol/min (adjusted $p < 0.01$). Significant (adjusted $p < 0.05$) OCR reductions were also shown by the noco 10 μM (42.26 ±14.52 pmol/min) and noco 50 μM (42.00 ± 11.19 pmol/min) groups, with a lower (2 μM) noco exposure leading to OCR reductions which trended toward but did not achieve significance (45.51 ± 11.97 pmol/min). In the case of cytD, 200 nM (51.69 ± 19.05 pmol/min) and 1 μM (49.13 ± 15.36 pmol/min) exposures decreased the basal OCR without achieving significance, but 5 μM left it unchanged (60.00 ± 12.21 pmol/min). Similarly, cells treated with noco 10 μM + cytD 1 μM only slightly decreased the basal OCR (55.78 ± 11.86 pmol/min) without achieving statistical significance.

Interestingly, any differences in OCR from control cells caused by cytoskeletal toxins are diminished under the effects of oligo, showing that proton leak is the same across control and experimental groups. Similarly, FCCP blurs basal OCR distinctions between experimental and control groups, suggesting that maximal respiration is largely preserved under the influence of cytoskeletal toxicity.

Increased intracellular calcium sensitizes cells to decreases in respiration induced by cytoskeletal inhibitors

Based on our initial results showing OCR decreases in response to cytoskeletal toxins, we hypothesized that cytoskeletal toxins sensitized cells to further upsets in mitochondrial homeostasis. As such, we challenged the cells with 100 nM A23, a calcium ionophore, prior to addition of cytoskeletal toxins. A23 causes an increase in the intracellular calcium concentration, which is likely buffered by mitochondria and thus introduces another level of mitochondrial stress. The chosen concentration did not affect OCR when used alone (Figure 5(i)).

Cells pretreated with A23 and then subjected to any concentration of noco showed significant decreases in basal OCR (Figure 5(ii)). Basal OCRs were 30.87 ± 12.10 pmol/min

for the 2 μM group (adjusted $p < 0.01$), 33.31 ± 9.42 pmol/min for the 10 μM group (adjusted $p < 0.01$), and 26.69 ± 14.88 pmol/min for the 50 μM group (adjusted $p < 0.001$). As in the group without A23 exposure, cells treated with A23 followed by noco 50 μM + cytD 5 μM showed significantly decreased OCRs of 29.28 ± 10.90 pmol/min (Figure 5(iv); adjusted $p < 0.01$). The A23 groups which differed most from their corresponding groups lacking A23 were cells exposed to cytD and noco 10 μM + cytD 1 μM. In the former groups, basal respiration is decreased in cells pretreated with A23 and then exposed to 200 nM cytD (37.41 ± 10.18 pmol/min; adjusted $p < 0.05$) or 1 μM cytD (33.24 ± 15.25 pmol/min; adjusted $p < 0.01$). Similarly, cells treated with noco 10 μM + cytD 1 μM showed decreased basal OCR only when pretreated with A23 (37.36 ± 14.57 pmol/min; adjusted $p < 0.05$). Cells in the 5 μM cytD group showed a slight decrease in basal respiration with A23 pre-treatment (50.27 ± 12.80 pmol/min), but this change did not achieve significance.

OCR decreases in experimental groups somewhat carried over to maximal respiration, and the adjusted p-values achieved significance ($p < 0.05$) for noco 2 μM, noco 50 μM, cytD 200 nM, cytD 1 μM, and noco 50 μM + cytD 5 μM (Figure 5). However, the differences between control and experimental groups were overall less extreme for maximal respiration than for basal respiration.

Cell viability was assessed in a separate group of experiments using PI staining after treatment. Only groups with the highest doses of drug, with and without A23, were tested (high DMSO ± A23, noco 50 μM ± A23, cytD 5 μM ± A23, noco 50 μM + cytD 5 μM ± A23). The results correlated with respiration measurements, with cells in the noco 50 μM ± A23 and noco 50 μM + cytD 5 μM ± A23 groups, but not the others, showing increased PI staining 3 hours after treatment (Figure 6). PI staining was spatially correlated with the appearance of floating cells in brightfield images. Importantly, PI staining did not appreciably increase in these groups after 30 minutes of treatment, the time around which basal respiration was measured.

DISCUSSION

This work establishes that cytoskeletal toxins alone can affect mitochondrial bioenergetics in fibroblasts. These findings differ from previous work in endothelial cells, which demonstrated reduced oxygen utilization in response to these toxins only when lactate dehydrogenase (LDH) was inhibited [30], likely connected to the glycolytic reliance of these cells [31]. Table 1 summarizes the results of our current work along with our previous findings on the effects of cytoskeletal toxins on mitochondrial motility [16]. In all cases, we did not see mitochondrial inner membrane depolarization within 30 minutes of treatment with cytoskeletal toxins, indicating that mitochondrial function is not drastically compromised. However, microtubule depolymerization via noco significantly reduced basal respiration in intact cells, an effect which was exacerbated when cells were pretreated with A23. This correlated with decreased mitochondrial motility in these cells [16]. CytD alone (200 nM and 1 μM) did not significantly affect either motility or respiration, but led to decreased basal OCR when cells were preconditioned with A23. The combined effects of actin depolymerization and increased calcium handling may thus present too great of a metabolic challenge for basal respiration to be maintained, although respiration maintenance

following 5 μM cytD + A23 suggests that effects depend on toxin concentration. The drastic reduction in basal OCR following severe depolymerization of both microtubules and microfilaments without A23 treatment (5 μM cytD + 50 μM noco) indicates an additive energetic consequence of these drugs. Interestingly, these cells show mitochondrial motility similar to controls [16], implying that changes in mitochondrial function are not necessarily reflected in altered mitochondrial motility.

Two particular treatment groups showed decreases in mitochondrial lengths: 5 μM cytD and 10 μM noco + 1 μM cytD. The maintenance of basal OCR in these cells suggests a connection between respiration rates and mitochondrial shortening, which is discussed further below. The lack of shortening in the 5 μM cytD + 50 μM noco group, concurrent with decreased basal OCR, further supports this link. The 5 μM cytD and 10 μM noco + 1 μM cytD groups differ in mitochondrial motility, which is increased by 5 μM cytD and decreased by 10 μM noco + 1 μM cytD. Additionally, A23 preconditioning does sensitize cells treated with 10 μM noco + 1 μM cytD, but not 5 μM cytD, to basal OCR reduction. Whether mitochondrial motility, which is increased by 5 μM cytD but decreased by 10 μM noco + 1 μM cytD, is related to this distinction is worthy of further study.

While cell death correlated with decreases in basal respiration, our results suggest that decreased respiration precedes cell death rather than the reverse. Little cell death was observed 30 minutes following treatment with noco 50 μM ± A23 or noco 50 μM + cytD 5 μM ± A23, despite basal respiration showing significant decreases at this point (Figure 6). More cell death and detachment were observed at the 3 hour time point, likely resulting from either decreased respiration or other ramifications of cytoskeletal collapse. Decreases in maximal respiration, which is measured in between the 30-minute and 3-hour time points of PI visualization, may reflect some cell death.

We did not observe any evidence of A23 itself influencing mitochondrial function. A23 acts as a general calcium ionophore in cells. Increases in cytosolic calcium are generally followed by increases in mitochondrial calcium (e.g. [34], reviewed by [35]), which can stimulate dehydrogenases of the tricarboxylic acid cycle and increase ATP production at low levels [35]. At sustained high concentrations, however, continual calcium accumulation into the mitochondrial matrix can uncouple respiration [36–39] or initiate cell death via opening of the mitochondrial permeability transition pore [35]. We first performed experiments using higher A23 concentrations (2 μM) which resulted in OCR changes without the addition of cytoskeletal toxins, confirming that A23 alone can affect mitochondrial function. We lowered the A23 concentration to 100 nM, which did not alter mitochondrial respiration (Figure 5(i)), and seemingly stressed the mitochondria just enough to sensitize them to further energetic upset.

Similarly, we do not expect that the concentration of A23 used affected mitochondrial respiration by exacerbating the cytoskeletal effects of the drugs used. Studies showing more global effects of A23 caused by severe disturbances in calcium regulation [40,41], including actin disintegration [42] and microtubule breakdown [43], used A23 concentrations one or more orders of magnitude greater than our 100 nM concentration. More significantly, the lack of OCR change using A23 alone as well as the additive effects on basal OCR of A23 to

cytD and noco concentrations which alone cause extreme depolymerization [16] suggest that A23 does not decrease mitochondrial OCR by affecting cytoskeletal structure. Rather, it seems to induce a distinct and perhaps more direct stress on mitochondrial function which emerges when mitochondria are further stressed by cytoskeletal depolymerization.

In all experimental groups, FCCP application blurs the distinction in OCR between control and treated groups, suggesting that mitochondrial capacity is largely maintained. Thus, lowered basal respiration is likely either an elective strategy to preserve energy in response to cytoskeletal inhibition, or an indication that energy is no longer needed to maintain the cytoarchitecture through continuous turnover of actin/tubulin monomers and polymers. Elective OCR reductions may still be harmful to the cell and be associated with increased cell death, as shown by the noco 50 μM and noco 50 μM + cytD 5 μM groups (Figure 6). Decreased energetic requirements of cytoskeletal maintenance may underlie the basal OCR decreases observed in the noco 10 μM, noco 50 μM and noco 50 μM + cytD 5 μM groups. However, the A23 experiments suggest that decreased energetic requirements of cytoskeletal maintenance do not contribute in the cases of cytD (200 nM-1 μM) or noco 10 μM + cytD 1 μM, since basal respiration is only significantly reduced when calcium regulation is altered by A23 in addition to cytoskeletal breakdown. Reduced maximal respiration in response to 200 nM and 1 μM cytD in A23-pretreated cells indicates that mitochondrial capacity is decreased by this cocktail of treatments, but this reduction is less extreme than the decrease in basal OCR in these groups. Unlike cytD-treated cells, noco-treated cells show compromised basal OCR without A23 pre-treatment, which is further decreased when cells are pretreated with A23. The aggravated effect following A23 pretreatment suggests some element of change in mitochondrial function which is independent of the energetic requirements of microtubule organization. Moreover, these cells show decreased maximal OCRs which trend toward or achieve significance, suggesting that mitochondrial respiration is impaired when both calcium and microtubule maintenance are disturbed. It is likely that some cell death contributes to the maximal respiration decrease, which is measured sometime between the 30-minute and 3-hour time points when PI staining was examined. Again, though, the FCCP-induced decreases are less extreme than decreases in basal respiration, indicating a combined effect of impaired mitochondrial function/cell death and elective energetic conservation.

The effects of cytoskeletal inhibitors on mitochondrial morphology vary by study. De Vos et al. did not see mitochondrial fragmentation following cytD treatment [44], while another study showed extreme mitochondrial fragmentation following 50 uM cytochalasin B or 10 uM noco in transfected epithelial cells [45]. Our observation that shortening occurs only in the 5 μM cytD and 10 μM noco + 1 μM cytD groups suggests that this response is highly specific.

The decrease in mitochondrial lengths observed in the 5 μM cytD and 10 μM noco + 1 μM cytD groups can either be caused by fragmentation or shortening of mitochondria. While numbers of mitochondria do increase following treatment (Figure S1), control cells exhibit a similar change. As such, mitochondria in treated cells do not appear to fragment to a greater degree than those in control cells. We do not expect that defective mitochondria resulting from fragmentation are lysed in the 30 minute duration of the experiment, so the numbers of

mitochondria detected at 30 minutes should be a true reflection of the effects of cytoskeletal inhibitors on mitochondrial number. We therefore conclude that the length decrease exhibited by mitochondria in these treatment groups is likely indicative of shortening rather than fragmentation. Most discussion in the literature pertaining to decreases in mitochondrial length relates to mitochondrial fission rather than shortening, with many studies observing mitochondrial fragmentation when mitochondrial energetics are severely impaired [46] and as a sign of apoptosis [47,48]. However, more recent work suggests that mitochondrial fragmentation may actually benefit the cell as a mechanism of eliminating dysfunctional mitochondria [49]. Several studies relate mitochondrial shortening without concurrent proportional increases in number of mitochondria. Examples include fibroblasts of patients with complex I deficiency [50] or neurons subjected to complex I inhibitors [51]. This phenomenon is overall less studied than mitochondrial fragmentation, and may represent an entirely different effect [51].

The two-dimensional imaging used for these experiments precluded definitive assessments as to whether mitochondrial shortening was indicative of changes in cell volume. However, multiplying normalized mitochondrial area by normalized number of mitochondria in a given cell should provide a two-dimensional estimate of change in mitochondrial “area” per cell. Beyond two-dimensionality, this strategy is additionally limited in its predictive ability because mitochondria were artificially “thickened” during image processing. Nonetheless, we found that cells in the control, 10 μM noco + 1 μM cytD and 5 μM cytD groups showed total mitochondrial areas of 122 ±25%, 92 ± 16% and 81 ± 14%, respectively, compared to before treatment. The latter two groups had the smallest metrics of total mitochondrial area among all groups tested, although two other groups had metric in the same range, likely resulting from the combined effects of smaller decreases in mitochondrial number and area compared to controls. While not providing definitive evidence of loss of mitochondrial volume, these preliminary results suggest that mitochondrial shortening observed in the 10 μM noco + 1 μM cytD and 5 μM cytD groups might be accompanied by decreased mitochondrial volume although not fragmentation per se.

In the present study, the concurrent observation of mitochondrial shortening with preserved basal OCR may have one of several mechanistic indications. As a cause, mitochondrial shortening may represent a protective mechanism that works to prevent cells from reducing respiration rates following severe cytoskeletal impairment. Alternatively, mitochondrial shortening may be an adverse effect of failure to decrease OCR in the face of severe cytoskeletal breakdown. In either case, the reduction of basal OCR in cells preconditioned with A23 and then treated with 10 μM noco + 1 μM cytD suggests that cells exposed to this cocktail of cytoskeletal toxins cannot maintain normal respiration rates when their mitochondria are already stressed by increased demands of calcium maintenance. The combination of A23 and 5 μM cytD, on the other hand, does not result in a reduction of basal OCR, suggesting that calcium-induced stress does not add to the effects of severe disintegration of actin alone. In either case, the interaction between mitochondrial shortening and respiration in these two groups seems to represent an entirely different energetic mechanism than reductions in basal OCR shown in other treatment groups, and merits further mechanistic study.

CONCLUSION

This study overall demonstrates that cytoskeletal impairment directly affects mitochondrial function in fibroblasts. Microtubule disintegration leads to decreased basal respiration which is exacerbated when mitochondria are additionally stressed with elevated calcium levels. On the other hand, actin depolymerization only affects mitochondrial respiration under conditions of disturbed calcium homeostasis. Mitochondrial shortening occurs in specific cases when respiration rates remain unchanged, suggesting an interplay between mitochondrial morphology and respiration. A systematic study of the interplay between cytoskeletal depolymerization and calcium homeostasis as affected by low A23 concentrations may elucidate the mechanisms underlying these findings. Additional experiments using inhibitors of mitochondrial fission may also confirm the potential protective effects of mitochondrial shortening on energetic maintenance in the cell, despite a majority of studies associating mitochondrial fragmentation with dysfunction. If the mitochondrial shortening we observe is operating by the same mechanisms as mitochondrial fission, then inhibiting fission may cause reduced basal OCR in cases when shortening appears to be protective.

Investigating the direct effects of cytoskeletal breakdown on mitochondrial respiration in fibroblasts demonstrates that cytoskeletal toxicity at times directly leads to reduced mitochondrial oxygen consumption in these cells, but more pervasively sensitizes them to further energetic insult. Beyond indicating a functional connection between mitochondria and the cytoskeleton, this work suggests that cells with distorted cytostructures lead to changes in cellular metabolism which may contribute to altered or compromised function. Relevant examples include migrating or dividing cells, which show temporary changes in their cytoarchitecture, as well as cancer cells or cells from patients exhibiting cardiovascular disease, which show permanent mechanical changes.

Supplementary Material

Refer to Web version on PubMed Central for supplementary material.

ACKNOWLEDGEMENTS

Thank you to Peter Sobolewski, Ph.D. for initial training in mitochondrial imaging and to Benjamin Kandel for help with image processing, statistical analyses and general manuscript feedback. Martha E. Grady, Ph.D. also provided valuable suggestions regarding manuscript preparation. We additionally thank Marni Falk, M.D. for general guidance and feedback regarding mitochondrial experimentation.

This work was funded by the Office of Naval Research grant N000141612100 (awarded to DME) and the National Institutes of Health grants NS021328 and CA182384 (awarded to DCW).

WORKS CITED

1. Warburg O. The metabolism of carcinoma cells. J Cancer Res. 1925; 9:148–163.
2. Trushina, E.; Dutta, T.; Persson, X-MT.; Mielke, MM.; Petersen, RC. Identification of Altered Metabolic Pathways in Plasma and CSF in Mild Cognitive Impairment and Alzheimer's Disease Using Metabolomics. In: Mufson, E., editor. PLoS ONE. Vol. 8. 2013. p. e63644doi:10.1371/journal.pone.0063644

3. Wiegman CH, Michaeloudes C, Haji G, Narang P, Clarke CJ, Russell KE, et al. Oxidative stress–induced mitochondrial dysfunction drives inflammation and airway smooth muscle remodeling in patients with chronic obstructive pulmonary disease. J Allergy Clin Immunol. 2015; 136:769–780. doi:10.1016/j.jaci.2015.01.046. [PubMed: 25828268]

4. Ryan BJ, Lourenço-Venda LL, Crabtree MJ, Hale AB, Channon KM, Wade-Martins R. α-Synuclein and mitochondrial bioenergetics regulate tetrahydrobiopterin levels in a human dopaminergic model of Parkinson disease. Free Radic Biol Med. 2014; 67:58–68. doi:10.1016/j.freeradbiomed.2013.10.008. [PubMed: 24148766]

5. Mackenzie RM, Salt IP, Miller WH, Logan A, Ibrahim HA, Degasperi A, et al. Mitochondrial reactive oxygen species enhance AMP-activated protein kinase activation in the endothelium of patients with coronary artery disease and diabetes. Clin Sci. 2013; 124:403–411. doi:10.1042/CS20120239. [PubMed: 23057846]

6. Knott AB, Perkins G, Schwarzenbacher R, Bossy-Wetzel E. Mitochondrial fragmentation in neurodegeneration. Nat Rev Neurosci. 2008; 9:505–518. doi:10.1038/nrn2417. [PubMed: 18568013]

7. Makino A, Scott BT, Dillmann WH. Mitochondrial fragmentation and superoxide anion production in coronary endothelial cells from a mouse model of type 1 diabetes. Diabetologia. 2010; 53:1783–1794. doi:10.1007/s00125-010-1770-4. [PubMed: 20461356]

8. Wang X, Winter D, Ashrafi G, Schlehe J, Wong YL, Selkoe D, et al. PINK1 and Parkin Target Miro for Phosphorylation and Degradation to Arrest Mitochondrial Motility. Cell. 2011; 147:893–906. doi:10.1016/j.cell.2011.10.018. [PubMed: 22078885]

9. Giedt RJ, Pfeiffer DR, Matzavinos A, Kao C-Y, Alevriadou BR. Mitochondrial Dynamics and Motility Inside Living Vascular Endothelial Cells: Role of Bioenergetics. Ann Biomed Eng. 2012; 40:1903–1916. doi:10.1007/s10439-012-0568-6. [PubMed: 22527011]

10. Kheradmand F. Role of Rac1 and Oxygen Radicals in Collagenase-1 Expression Induced by Cell Shape Change. Science. 1998; 280:898–902. doi:10.1126/science.280.5365.898. [PubMed: 9572733]

11. Munevar S, Wang Y, Dembo M. Traction force microscopy of migrating normal and H-ras transformed 3T3 fibroblasts. Biophys J. 2001; 80:1744–1757. [PubMed: 11259288]

12. Jalil JE, Doering CW, Janicki JS, Pick R, Shroff SG, Weber KT. Fibrillar collagen and myocardial stiffness in the intact hypertrophied rat left ventricle. Circ Res. 1989; 64:1041–1050. doi:10.1161/01.RES.64.6.1041. [PubMed: 2524288]

13. Levental KR, Yu H, Kass L, Lakins JN, Egeblad M, Erler JT, et al. Matrix Crosslinking Forces Tumor Progression by Enhancing Integrin Signaling. Cell. 2009; 139:891–906. doi:10.1016/j.cell.2009.10.027. [PubMed: 19931152]

14. Sehgel NL, Zhu Y, Sun Z, Trzeciakowski JP, Hong Z, Hunter WC, et al. Increased vascular smooth muscle cell stiffness: a novel mechanism for aortic stiffness in hypertension. AJP Heart Circ Physiol. 2013; 305:H1281–H1287. doi:10.1152/ajpheart.00232.2013.

15. Li QS, Lee GYH, Ong CN, Lim CT. AFM indentation study of breast cancer cells. Biochem Biophys Res Commun. 2008; 374:609–613. doi:10.1016/j.bbrc.2008.07.078. [PubMed: 18656442]

16. Kandel J, Chou P, Eckmann DM. Automated detection of whole-cell mitochondrial motility and its dependence on cytoarchitectural integrity: Global Analysis of Mitochondrial Motility. Biotechnol Bioeng. 2015; 112:1395–1405. doi:10.1002/bit.25563. [PubMed: 25678368]

17. Ball EH, Singer SJ. Mitochondria are associated with microtubules and not with intermediate filaments in cultured fibroblasts. Proc Natl Acad Sci U S A. 1982; 79:123–126. [PubMed: 6275382]

18. Morris RL, Hollenbeck PJ. Axonal transport of mitochondria along microtubules and F-actin in living vertebrate neurons. J Cell Biol. 1995; 131:1315–1326. [PubMed: 8522592]

19. Janmey PA, McCulloch CA. Cell mechanics: integrating cell responses to mechanical stimuli. Annu Rev Biomed Eng. 2007; 9:1–34. doi:10.1146/annurev.bioeng.9.060906.151927. [PubMed: 17461730]

20. Lazzarino DA, Boldogh I, Smith MG, Rosand J, Pon LA. Yeast mitochondria contain ATP-sensitive, reversible actin-binding activity. Mol Biol Cell. 1994; 5:807–818. doi:10.1091/mbc.5.7.807. [PubMed: 7812049]

21. Korobova F, Ramabhadran V, Higgs HN. An Actin-Dependent Step in Mitochondrial Fission Mediated by the ER-Associated Formin INF2. Science. 2013; 339:464–467. doi:10.1126/science.1228360. [PubMed: 23349293]
22. Morris RL, Hollenbeck PJ. The regulation of bidirectional mitochondrial transport is coordinated with axonal outgrowth. J Cell Sci. 1993; 104(Pt 3):917–927. [PubMed: 8314882]
23. Rojo G, Chamorro M, Salas ML, Viñuela E, Cuezva JM, Salas J. Migration of mitochondria to viral assembly sites in African swine fever virus-infected cells. J Virol. 1998; 72:7583–7588. [PubMed: 9696857]
24. Bereiter-Hahn, J. International Review of Cytology. Elsevier; 1990. Behavior of Mitochondria in the Living Cell; p. 1-63.Available: http://linkinghub.elsevier.com/retrieve/pii/S007476960861205X
25. Bereiter-Hahn J, Lück M, Miebach T, Stelzer HK, Vöth M. Spreading of trypsinized cells: cytoskeletal dynamics and energy requirements. J Cell Sci. 1990; 96(Pt 1):171–188. [PubMed: 2373741]
26. Johnson LV. Monitoring of relative mitochondrial membrane potential in living cells by fluorescence microscopy. J Cell Biol. 1981; 88:526–535. doi:10.1083/jcb.88.3.526. [PubMed: 6783667]
27. Collins TJ, Berridge MJ, Lipp P, Bootman MD. Mitochondria are morphologically and functionally heterogeneous within cells. EMBO J. 2002; 21:1616–1627. doi:10.1093/emboj/21.7.1616. [PubMed: 11927546]
28. Campello S, Lacalle RA, Bettella M, Manes S, Scorrano L, Viola A. Orchestration of lymphocyte chemotaxis by mitochondrial dynamics. J Exp Med. 2006; 203:2879–2886. doi:10.1084/jem.20061877. [PubMed: 17145957]
29. Desai SP, Bhatia SN, Toner M, Irimia D. Mitochondrial localization and the persistent migration of epithelial cancer cells. Biophys J. 2013; 104:2077–2088. doi:10.1016/j.bpj.2013.03.025. [PubMed: 23663851]
30. Tillmann U, Bereiter-Hahn J. Relation of actin fibrils to energy metabolism of endothelial cells. Cell Tissue Res. 1986; 243 doi:10.1007/BF00218065.
31. Culic O, Gruwel ML, Schrader J. Energy turnover of vascular endothelial cells. Am J Physiol. 1997; 273:C205–213. [PubMed: 9252458]
32. Sauvanet C, Duvezin-Caubet S, di Rago J-P, Rojo M. Energetic requirements and bioenergetic modulation of mitochondrial morphology and dynamics. Semin Cell Dev Biol. 2010; 21:558–565. doi:10.1016/j.semcdb.2009.12.006. [PubMed: 20025987]
33. Perry S, Norman J, Barbieri J, Brown E, Gelbard H. Mitochondrial membrane potential probes and the proton gradient: a practical usage guide. BioTechniques. 2011; 50:98–115. doi:10.2144/000113610. [PubMed: 21486251]
34. Sobolewski, P.; Kandel, J.; Eckmann, DM. Air Bubble Contact with Endothelial Cells Causes a Calcium-Independent Loss in Mitochondrial Membrane Potential. In: Grundmann, S., editor. PLoS ONE. Vol. 7. 2012. p. e47254doi:10.1371/journal.pone.0047254
35. Finkel T, Menazza S, Holmstrom KM, Parks RJ, Liu J, Sun J, et al. The Ins and Outs of Mitochondrial Calcium. Circ Res. 2015; 116:1810–1819. doi:10.1161/CIRCRESAHA.116.305484. [PubMed: 25999421]
36. Reed PW, Lardy HA. A23187: a divalent cation ionophore. J Biol Chem. 1972; 247:6970–6977. [PubMed: 4263618]
37. Wong DT, Wilkinson JR, Hamill RL, Horng J-S. Effects of antibiotic lonophore, A23187, on oxidative phosphorylation and calcium transport of liver mitochondria. Arch Biochem Biophys. 1973; 156:578–585. doi:10.1016/0003-9861(73)90308-1. [PubMed: 4268878]
38. Lemasters JJ, Nieminen AL, Qian T, Trost LC, Herman B. The mitochondrial permeability transition in toxic, hypoxic and reperfusion injury. Mol Cell Biochem. 1997; 174:159–165. [PubMed: 9309681]
39. Petronilli V, Penzo D, Scorrano L, Bernardi P, Di Lisa F. The Mitochondrial Permeability Transition, Release of Cytochrome c and Cell Death. CORRELATION WITH THE DURATION OF PORE OPENINGS IN SITU. J Biol Chem. 2001; 276:12030–12034. doi:10.1074/jbc.M010604200. [PubMed: 11134038]

40. White JG, Rao GH, Gerrard JM. Effects of the lonophore A23187 on blood platelets I. Influence on aggregation and secretion. Am J Pathol. 1974; 77:135–149. [PubMed: 4374890]
41. Kim M-J, Jo D-G, Hong G-S, Kim BJ, Lai M, Cho D-H, et al. Calpain-dependent cleavage of cain/cabin1 activates calcineurin to mediate calcium-triggered cell death. Proc Natl Acad Sci. 2002; 99:9870–9875. doi:10.1073/pnas.152336999. [PubMed: 12114545]
42. Kuhne W, Besselmann M, Noll T, Muhs A, Watanabe H, Piper HM. Disintegration of cytoskeletal structure of actin filaments in energy-depleted endothelial cells. Am J Physiol. 1993; 264:H1599–1608. [PubMed: 8388659]
43. Lieuvin A, Labbé JC, Dorée M, Job D. Intrinsic microtubule stability in interphase cells. J Cell Biol. 1994; 124:985–996. [PubMed: 8132719]
44. De Vos KJ, Allan VJ, Grierson AJ, Sheetz MP. Mitochondrial Function and Actin Regulate Dynamin-Related Protein 1-Dependent Mitochondrial Fission. Curr Biol. 2005; 15:678–683. doi:10.1016/j.cub.2005.02.064. [PubMed: 15823542]
45. Kumemura H, Harada M, Yanagimoto C, Koga H, Kawaguchi T, Hanada S, et al. Mutation in keratin 18 induces mitochondrial fragmentation in liver-derived epithelial cells. Biochem Biophys Res Commun. 2008; 367:33–40. doi:10.1016/j.bbrc.2007.12.116. [PubMed: 18164256]
46. Benard G, Bellance N, James D, Parrone P, Fernandez H, Letellier T, et al. Mitochondrial bioenergetics and structural network organization. J Cell Sci. 2007; 120:838–848. doi:10.1242/jcs.03381. [PubMed: 17298981]
47. Olichon A. Loss of OPA1 Perturbates the Mitochondrial Inner Membrane Structure and Integrity, Leading to Cytochrome c Release and Apoptosis. J Biol Chem. 2003; 278:7743–7746. doi:10.1074/jbc.C200677200. [PubMed: 12509422]
48. Jagasia R, Grote P, Westermann B, Conradt B. DRP-1-mediated mitochondrial fragmentation during EGL-1-induced cell death in C. elegans. Nature. 2005; 433:754–760. doi:10.1038/nature03316. [PubMed: 15716954]
49. Twig G, Elorza A, Molina AJA, Mohamed H, Wikstrom JD, Walzer G, et al. Fission and selective fusion govern mitochondrial segregation and elimination by autophagy. EMBO J. 2008; 27:433–446. doi:10.1038/sj.emboj.7601963. [PubMed: 18200046]
50. Koopman WJH, Visch H-J, Verkaart S, van den Heuvel LWPJ, Smeitink JAM, Willems PHGM. Mitochondrial network complexity and pathological decrease in complex I activity are tightly correlated in isolated human complex I deficiency. Am J Physiol Cell Physiol. 2005; 289:C881–890. doi:10.1152/ajpcell.00104.2005. [PubMed: 15901599]
51. Yuan H, Gerencser AA, Liot G, Lipton SA, Ellisman M, Perkins GA, et al. Mitochondrial fission is an upstream and required event for bax foci formation in response to nitric oxide in cortical neurons. Cell Death Differ. 2007; 14:462–471. doi:10.1038/sj.cdd.4402046. [PubMed: 17053808]

While mitochondria are known to be physically linked to microtubules, functional connections between mitochondria and the cytoskeleton are largely unexplored. We previously demonstrated that cytoskeletal toxicity alters mitochondrial motility in human fibroblasts. Here, we further characterize the mitochondrial effects of cytoarchitectural breakdown through quantitative approaches to fluorescence microscopy and metabolic assays. We show that cytoskeletal toxins can lead to decreases in mitochondrial oxygen consumption, and that intracellular calcium increases further sensitize mitochondria to this effect. Our results additionally suggest that decreased mitochondrial lengths correlate with maintenance of mitochondrial respiration. Underscoring causative connections between mitochondrial and cytoskeletal alterations may inform mechanisms underlying development of many diseases, such as cancer and cardiovascular disease, which feature dysfunction in both of these realms.

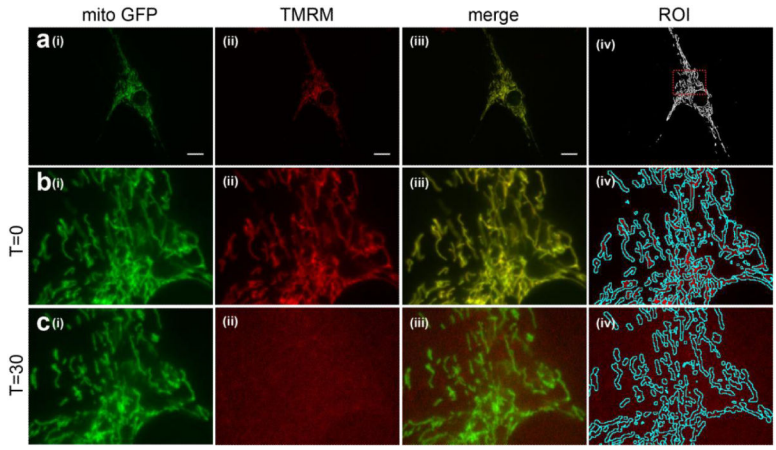

Figure 1. Measuring changes in mitochondrial morphology and inner membrane potential using fluorescence microscopy

Image of a sample cell co-stained with CellLight Mitochondria-GFP (mitoGFP) and TMRM. In all rows, (i) shows mitoGFP, (ii) shows TMRM and (iii) shows the two channels merged. (a) image of the entire cell before any drug treatment. (iv) shows the image resulting from ImageJ processing of the mitoGFP image in order to measure mitochondrial morphology and create a ROI for measuring mitochondrial inner membrane potential. The red dotted box indicates the area of the cell depicted in panels (b-c).(b-c) Magnified section of the cell prior to (b) and following (c) treatment with 5 μM CCCP. (iv) shows how the ROI resulting from the mitoGFP channel is overlaid onto the TMRM channel in order to measure TMRM fluorescence only within the mitochondria.

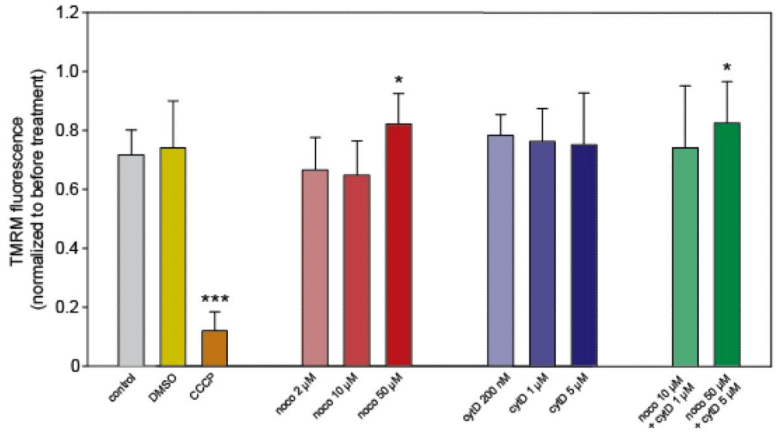

Figure 2. Mitochondrial potential remains unchanged following treatment with cytoskeletal toxins

Before drug treatment, cells were imaged in both the mitoGFP and TMRM channels. The mitoGFP channel was used to create a mitochondrial ROI which was then overlaid onto the TMRM image in order to measure fluorescence only within the mitochondria. The same procedure was repeated at 30 minutes following drug treatment, and resulting TMRM fluorescence for each was normalized to fluorescence for that cell prior to treatment. N=7-22 cells per group, each from a separate dish. * indicates an adjusted p-value of < 0.05, *** indicates adjusted $p < 0.001$ resulting from pairwise t-tests.

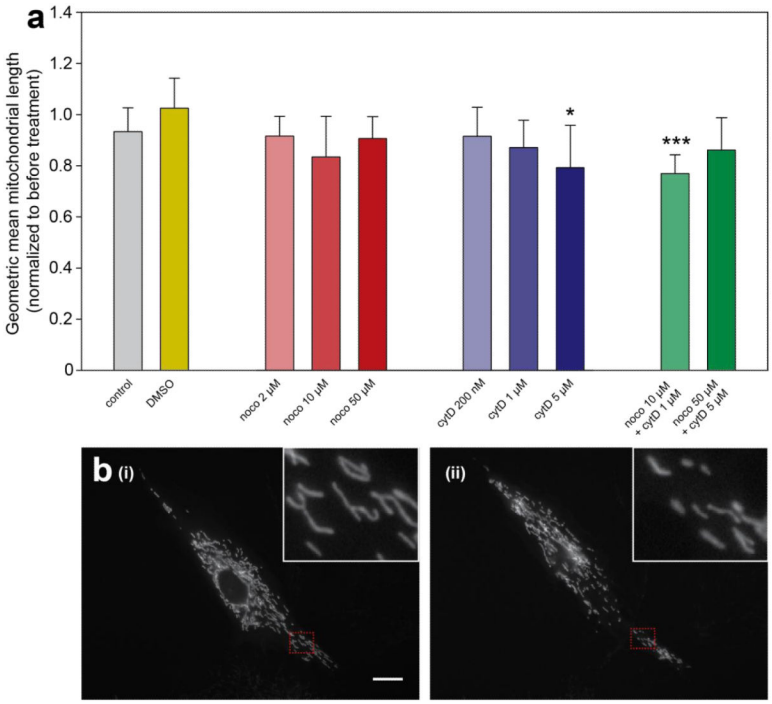

Figure 3. Specific cytoskeletal toxins induce shortening of mitochondria

(a) ImageJ was used to preprocess the mitoGFP image for each cell at each experimental time point. Matlab object recognition functions then measured physical characteristics of the mitochondria in the resulting image. Geometric means of mitochondrial lengths were calculated for each cell at each time point. Geometric mean length of mitochondria in a given cell at T=30 was then normalized to geometric mean length at T=0 for the same cell. N=8-22 cells per group. * indicates an adjusted p-value of < 0.05, *** indicates adjusted p <0.001 resulting from pairwise t-tests. (b) An example cell exhibiting mitochondrial shortening. (i) shows the cell prior to treatment, and (ii) shows the same cell at 30 minutes following treatment with 5 μM cytD. Red dotted lines indicate subcellular areas shown in the insets.

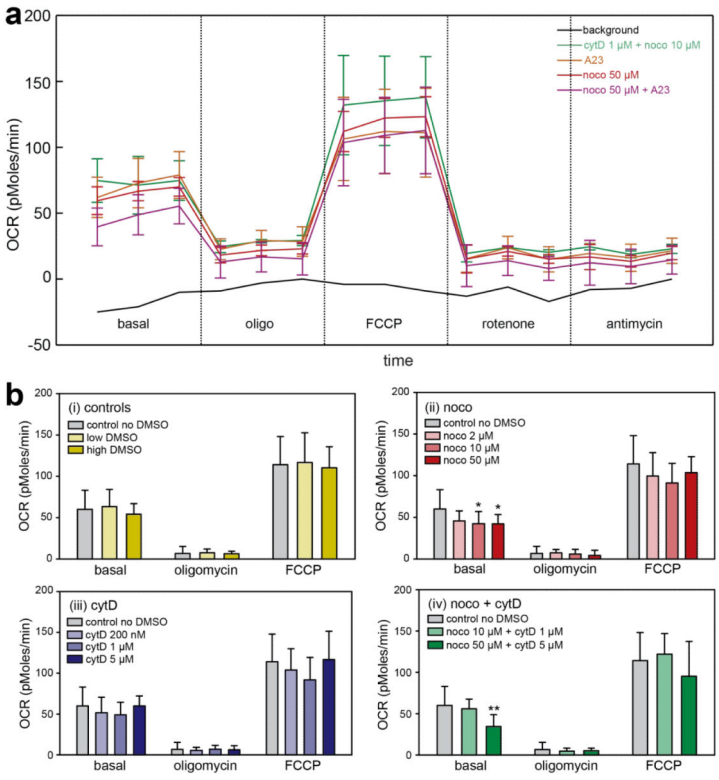

Figure 4. Influence of cytoskeletal inihibitors on basal oxygen consumption

(a) Sample oxygen consumption experiment. Each tracing represents the mean OCR readings from all wells in a given group (N=4-6 wells per group in a single experiment). Error bars show standard deviations for each group. Outliers have been omitted. Two of the three background wells in this case were outliers, so the background reading has no standard deviation. (b) Oxygen consumption rates for (i) control groups; (ii) groups treated with noco; (iii) groups treated with cytD; (iv) groups treated with both noco and cytD. The OCR from each well following antimycin addition has been subtracted prior to data analysis in order to consider only mitochondrial respiration. Bars represent means with error bars showing standard deviations. N=11-17 wells per group. *indicates $p < 0.05$; ** indicates $p < 0.01$.

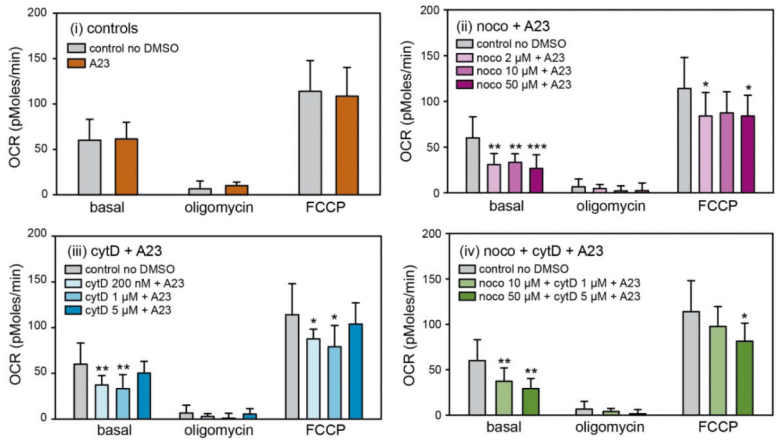

Figure 5. Cytoskeletal inhibitors sensitize cells to changes in calcium homeostasis, leading to decreased basal mitochondrial oxygen consumption rates

Oxygen consumption rates for cells treated with (i) A23 alone; (ii) noco and A23; (iii) cytD and A23; (iv) noco, cytD and A23. The OCR from each well following antimycin addition has been subtracted prior to data analysis in order to consider only mitochondrial respiration. Bars represent means with error bars showing standard deviations. N=12-17 wells per group. *indicates $p < 0.05$; ** indicates $p < 0.01$; *** indicates $p < 0.001$.

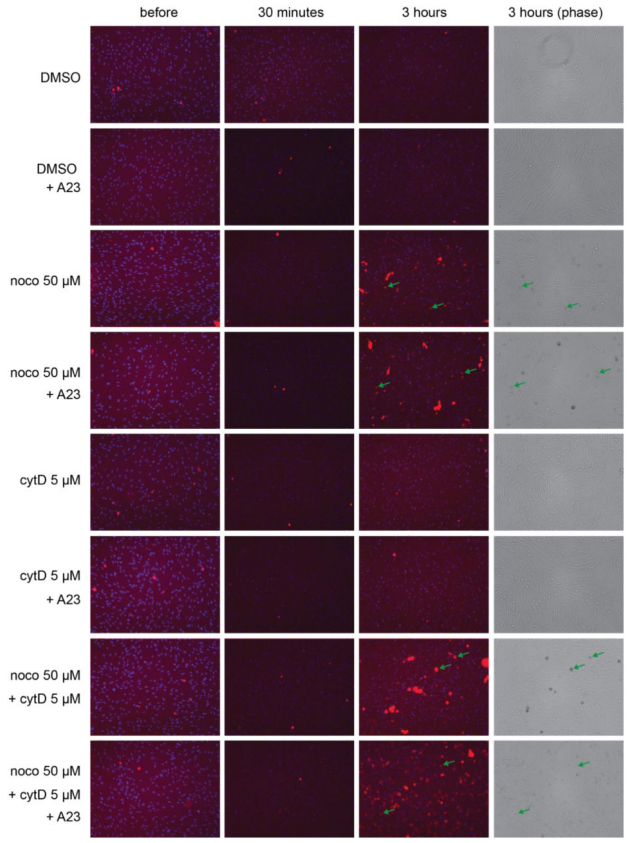

Figure 6. Viability of cells following highest doses of drug treatments

Cell nuclei are stained in blue with Hoechst, while red dye indicates PI staining. Representative images shown were taken at the same exposure at each time point and identically contrast enhanced for better visualization across all time points. Green arrows indicate rounded cells in both fluorescent and phase images.

Table 1

Summary of mitochondrial effects of cytoskeletal toxins

Group	Motility [16]	Length	OCR	OCR with A23
CytD 200 nM	--	--	--	↓ *
CytD 1 μM	--	--	--	↓ **
CytD 5 μM	↑	↓ *	--	--
Noco 2 μM	↓	--	--	↓ **
Noco 10 μM	↓	--	↓ *	↓ **
Noco 50 μM	↓	--	↓ *	↓ **
CytD 1 μM + Noco 10 μM	↓ #	↓ ***	--	↓ *
CytD 5 μM + Noco 50 μM	--	--	↓ **	↓ **

Results detailing our previous work on mitochondrial motility are shown in the “Motility” column. ↑ indicates an increase as compared to control, while ↓ indicates a decrease as compared to control.

* indicates adjusted $p < 0.05$,

** $p < 0.01$,

*** $p < 0.001$.

# indicates work which was previously performed but not published together with our earlier work on mitochondrial motility.